NANOMATERIALS

10.1126/sciadv.1500441

Total structure determination of surface doping $[Ag_{46}Au_{24}(SR)_{32}](BPh_4)_2$ nanocluster and its structure-related catalytic property

Shuxin Wang,* Shan Jin,* Sha Yang, Shuang Chen, Yongbo Song, Jun Zhang, Manzhou Zhu†

The structure effect is widely present in the catalysis of alloy systems. However, the surface structure of this system is still ambiguous because of the limitations of the current surface characterization tools. We reported the x-ray crystallographic structure of the first and the largest AgAu alloy nanocluster with a doping shell formulated as $[Ag_{46}Au_{24}(SR)_{32}](BPh_4)_2$. This nanocluster consists of an achiral bimetallic $Ag_2@Au_{18}@Ag_{20}$ core protected by a chiral $Ag_{24}Au_6(SR)_{32}$ shell. The catalysis experiments further revealed that the surface structure affects the selectivity of products significantly. This is the first case to find the structure effect in atomically precise alloy nanoclusters. Our work will benefit the basic understanding of bimetal distribution, as well as the structure-related catalytic property of alloy nanoclusters at the atomic level.

INTRODUCTION

Alloy nanoparticles have emerged as a new category of nanomaterials in recent years (*1*). These nanoparticles were widely applied across a diverse range of fields from catalysis to sensing and biolabeling (*2*–*12*). Recent research revealed that physical and chemical properties such as catalytic activity and selectivity (*13*–*17*) as well as electrical (*18*) and optical properties (*19*) are highly structure-dependent. Thus, uncovering the structures of nanoparticles is of extreme significance and has attracted intense research efforts. Thiolate-protected atomically precise Au or Ag nanoparticles (also called nanoclusters) represent an important class of noble metal nanoparticles due to precise determination of their structures. In the past few years, great improvement has been made in understanding the surface structures and metal packing modes of these nanoclusters by using x-ray crystallography (*20*). On the basis of these efforts, the structural construction and the related catalytic, magnetism, luminescence, and other properties of homogold or homosilver nanoclusters have been well studied (*20*–*33*). Compared to the homometal nanoclusters, the structures of bimetallic nanoclusters have been rarely investigated. Recently, three thiolate-protected Au-Ag nanoclusters have been successfully determined by x-ray crystallography (*34*–*36*). It is interesting to find that these alloy nanoclusters retain the same frameworks as their homometal counterparts with homometallic shells (*37*–*40*). This phenomenon raises questions such as whether alloy nanoclusters with doped surfaces exist or not and how the atoms are packing within these alloy nanoparticles. The unique surface structure may provide opportunities for a better understanding of packing modes of alloy nanoparticles and structure-related properties.

Herein, we accomplished surface doping in Ag-Au nanoclusters and obtained a chiral $[Ag_{46}Au_{24}(SR)_{32}](BPh_4)_2$ (R=^{t}Bu) nanocluster, which constitutes the largest bimetallic nanocluster structure thus far. The atomic structure of $[Ag_{46}Au_{24}(SR)_{32}](BPh_4)_2$ nanocluster can be described as a three-shelled achiral $Ag_2@Au_{18}@Ag_{20}$ core surrounded by a chiral bimetallic shell comprising of six heart-like units. The free valence electrons were calculated to 36 (70-32-2). The total structure of this thiolate-protected bimetallic nanocluster uncovers the unprecedented bimetallic Ag_2Au_1SR unit as well as the Ag_4SR unit as the unique surface-protecting motifs. This newly found surface doping $[Ag_{46}Au_{24}(SR)_{32}](BPh_4)_2$ bimetallic nanocluster provides an opportunity to study the packing mode and structure-related catalytic property in a bimetallic system at the atomic level.

RESULTS AND DISCUSSION

The structure of $[Ag_{46}Au_{24}(SR)_{32}]^{2+}$ nanocluster (counterion: two BPh_4^- ions) was solved by single-crystal x-ray crystallography (Fig. 1). The 70 metal atoms in this nanocluster are distributed in three shells. The central two silver atoms are surrounded by a tubbiness structure composed of 18 gold atoms (Fig. 2, A and B), which are capped with 20 silver atoms (Fig. 2, C and D). The 18 core gold atoms are distributed into three hexagons, and the overall shape resembles a barrel. Within this 18–gold atom shell, the average Au-Au distance is 2.7764 Å. The second shell consists of 20 silver atoms, with the top and bottom two silver atoms as covers of 18 core gold atoms. Among the remaining 18 silver atoms in the second shell, every six silver atoms form concentric hexagons with six gold atoms in the first shell. The average M-M distance in the $Ag_{20}Au_{18}$ core is 2.8821 Å. The $Ag_{20}Au_{18}$ core can also be considered as two types (types A and B) of layers (Fig. 2D): type A is one silver atom; type B is a hexagonal Au_6 with another six vertex caps (Ag_6). These two types of layers give rise to the 1:12:1:12:1:12:1 layers and can be described as nearly hexagonal close-packed A:B:A layering. Note that the similar 9:1:9 layer structure was also reported in $[Au_{39}(PPh_3)_{14}Cl_6]Cl_2$ by Teo *et al.* (*41*).

The $Ag_{22}Au_{18}$ core is protected by an Au-Ag bimetallic shell. The doped shell composition in our case can be seen as six eight–metal atom motifs $Ag_7Au_1(SR)_8$ resembling a "heart" shape, and each motif shares an $Ag_3(SR)_3$ unit with the neighboring two hearts (Fig. 2, E and F). Four types of bonding modes are found in this nanocluster (Fig. 2G): (i) One RS connects with three Ag atoms to form Ag_3SR, and this bonding mode is common in other thiolate-protected silver nanoclusters, such as Ag_{44} and Ag_{62} (*40*, *42*, *43*). (ii) One RS connects with four Ag atoms to form a Ag_4SR unit. The Ag-S distance in this unit is very unusual. For example, the distance of S-Ag_{core} bond was much shorter (2.330 Å) than

Department of Chemistry and Center for Atomic Engineering of Advanced Materials, Anhui University, Hefei, Anhui 230601, People's Republic of China.
*These authors contributed equally to this work.
†Corresponding author. E-mail: zmz@ahu.edu.cn

that of in Ag_{44} nanoclusters (~2.6 Å), indicating the strong interaction between Ag and RS groups. The two longer S-Ag_{shell} (2.911 and 2.950 Å) indicates the fairly weak bonding therein, which has never been previously reported in homosilver and bimetallic nanoclusters. (iii) One RS is bonded with two Ag atoms and one Au atom to form an Ag_2Au_1SR, and this mode is unique in the alloy nanocluster. In this context, this mode represents the first example to identify the capability of the thiolate group in forming the bimetallic surface. (iv) Staple-like $Au_1(SR)_2$, one Au atom, and two S atoms are almost on a line, similar to the bonding mode in $Au_{18}(SR)_{14}$, $Au_{23}(SR)_{16}$, $Au_{30}(SR)_{18}$, $Au_{102}(SR)_{44}$, and $Au_{133}(SR)_{52}$ nanoclusters (*44*–*50*).

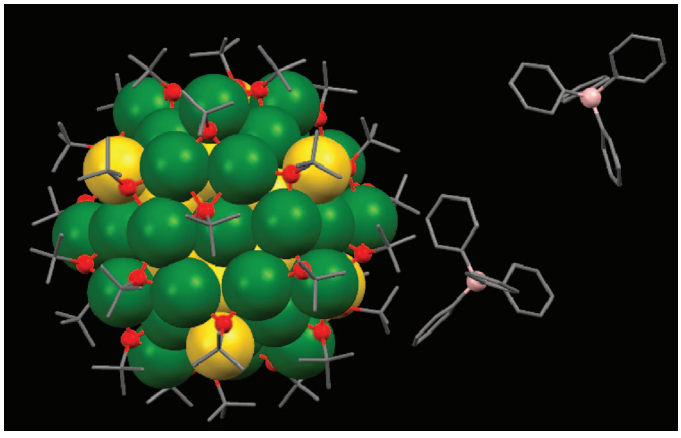

Fig. 1. Total structure of bimetallic chiral $[Ag_{46}Au_{24}(SR)_{32}](BPh_4)_2$ nanocluster (one of enantiomer) by x-ray crystallography. Gray, carbon; red, sulfur; green, silver; yellow, gold; pink, boron. The hydrogen atoms were omitted for clarity reasons.

The previously reported structures of Ag-Au alloy nanoclusters are based on the same framework of the same-sized homometal nanoclusters [for example, $Ag_{32}Au_{12}(SR)_{32}$ versus $Ag_{44}(SR)_{30}$ (*34*, *40*), $Ag_xAu_{38-x}(SR)_{24}$ versus $Au_{38}(SR)_{24}$ (*36*, *39*), and $Ag_xAu_{25-x}(SR)_{18}$ versus $Au_{25}(SR)_{18}$) (*35*, *37*, *38*)]. The same situation was also predicted in the case of $Ag_xAu_{144-x}(SR)_{60}$ nanoclusters (*51*). In these nanoclusters, the second metal could only be doped in the core, whereas the surface motifs are homometallic. By contrast, the $[Ag_{46}Au_{24}(SR)_{32}]^{2+}$ nanocluster represents the first example, which shows that silver and gold coexist in the surface motifs.

As shown in Fig. 2 (C and D), the metal core of this nanocluster is achiral. To further identify the origin of chirality in this nanocluster, we remove the metal core, the AuRS unit in the shell, as well as the top and bottom RS groups. As shown in Fig. 3A, the point group of a Ag-RS shell is D_{3d} after removing these groups, suggesting that this shell is achiral. The tilted AuSR units reduce the symmetry by eliminating three σ_d, with a symmetric center remaining (Fig. 3B). The top and bottom RS groups give rise to chirality (Fig. 3, C and D) in the $[Ag_{46}Au_{24}(SR)_{32}](BPh_4)_2$ nanocluster (Fig. 3, E and F). The findings on chirality in this nanocluster are remarkable. In general, two major effects might be responsible for the chiral of homometal nanoclusters: (i) the chiral ligands can induce the chiral of achiral nanoclusters (*52*) and (ii) asymmetric arrangement of an RS-Au-RS group on the achiral gold nanoclusters (*39*, *48*, *49*, *50*, *53*). In our case, asymmetric arrangement of the two RS groups changed the chirality of the nanoclusters.

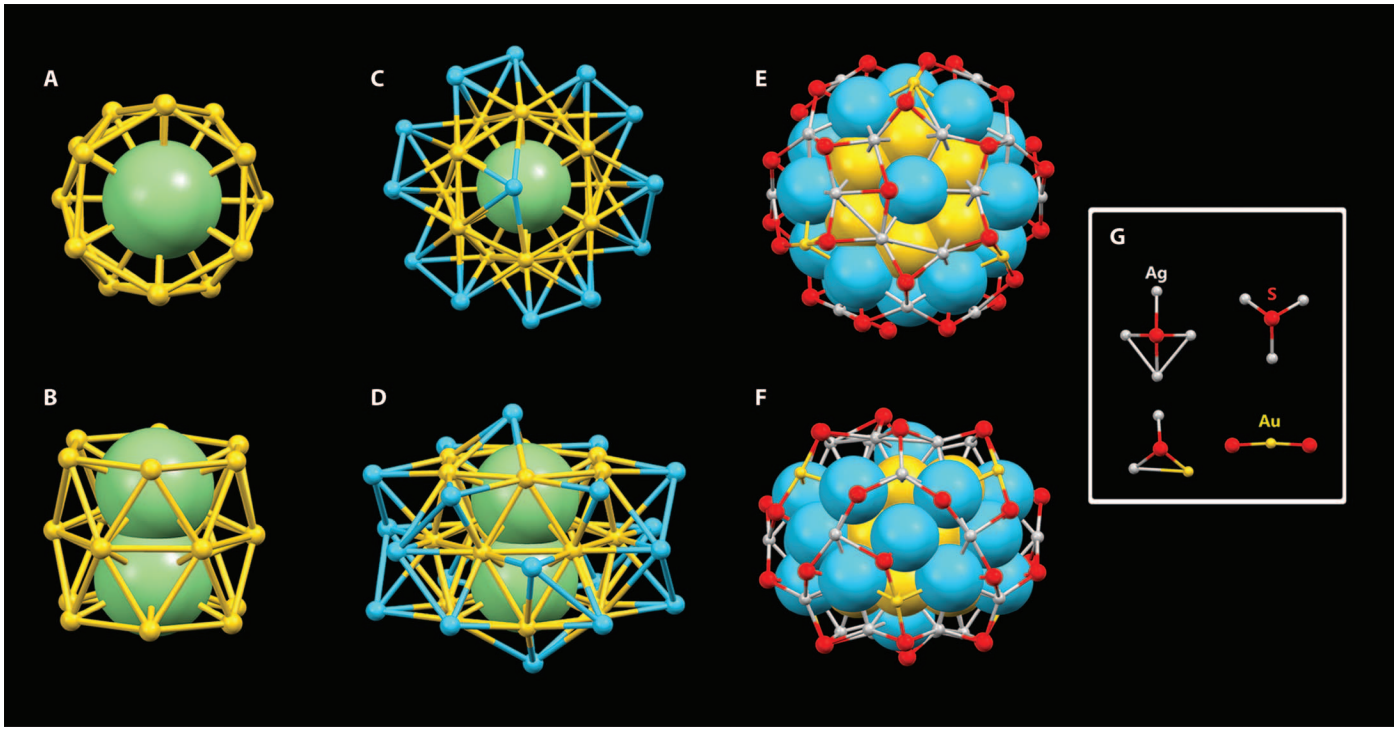

Fig. 2. The three-shell structure of $[Ag_{46}Au_{24}(SR)_{32}]^{2+}$. (**A** and **B**) Top and side $[Ag_{46}Au_{24}(SR)_{32}](BPh_4)_2$ views of the Ag_2Au_{18} core (which is not connected with any thiolate ligands). (**C** and **D**) Top and side views of the $Ag_2@Au_{18}@Ag_{20}$ core. (**E** and **F**) Top and side views of the $Ag_2@Au_{18}@Ag_{20}$ core protected by $Ag_{24}Au_6(SR)_{32}$ bimetallic shell. (**G**) Four bonding modes in the motif structure. Light green/blue/gray, silver; yellow, gold; red, sulfur.

The nanocluster formula and charge state were further confirmed by nuclear magnetic resonance (NMR) analysis (fig. S1). In the ^{1}H NMR spectrum of $[Ag_{46}Au_{24}(SR)_{32}](BPh_4)_2$, the peaks at 6.5 to 7.5 ppm (40 H) are assigned to $-C_6H_5$ of Ph_4B^-, and the peaks at 0.5 to 4.5 ppm (288.7 H) are assigned to $-CH_3$ in the $-SBu^t$ ligands. This result is consistent with the proton ratio (C_6H_5:CH_3=40:288) and thus indicates the 1:2 ratio of $Ag_{46}Au_{24}(SR)_{32}$ to Ph_4B^-, in agreement with the x-ray crystallographic result.

With the successfully determined $Ag_{46}Au_{24}(SR)_{32}$ nanocluster structure, a comparison with the previously reported core-shell structured Ag-Au bimetallic nanoclusters is now available. This could provide a simple model for understanding the structural effect in styrene oxidation catalyzed by the bimetallic silver-gold nanocluster.

We synthesized a series of structure-determined homometal and alloy nanoclusters, such as $Au_{25}(SR)_{18}$, $Ag_{44}(SR)_{30}$, $Ag_{32}Au_{12}(SR)_{30}$, and $Ag_{46}Au_{24}(SR)_{32}$ nanoclusters (see the Supplementary Materials for details). Multiwalled carbon nanotubes (CNTs) were used as the common carrier because of the fact that all of these nanoclusters can be efficiently adsorbed on the CNT surface. In addition, CNTs have an advantage to prevent diffusion of naked nanoclusters (*54*). Transmission electron microscopy (TEM) (figs. S2 and S3) showed that the clusters were evenly spread on CNTs and that all nanoclusters have average sizes of about 2 nm before and after reaction. This indicates negligible aggregation of clusters owing to sufficient interaction between the nanocluster and CNT (*9*).

Table 1 summarizes the results. Epoxide and benzaldehyde were the major products in the styrene oxidation. All catalysts showed high activity compared to plain CNT. Homogold Au_{25}/CNT showed the highest conversion of styrene, that is, 72.8%, whereas the selectivity for benzaldehyde is 66.4%. The homosilver Ag_{44}/CNT showed a much lower conversion (that is, 43.6%) than the homogold nanocluster did but it

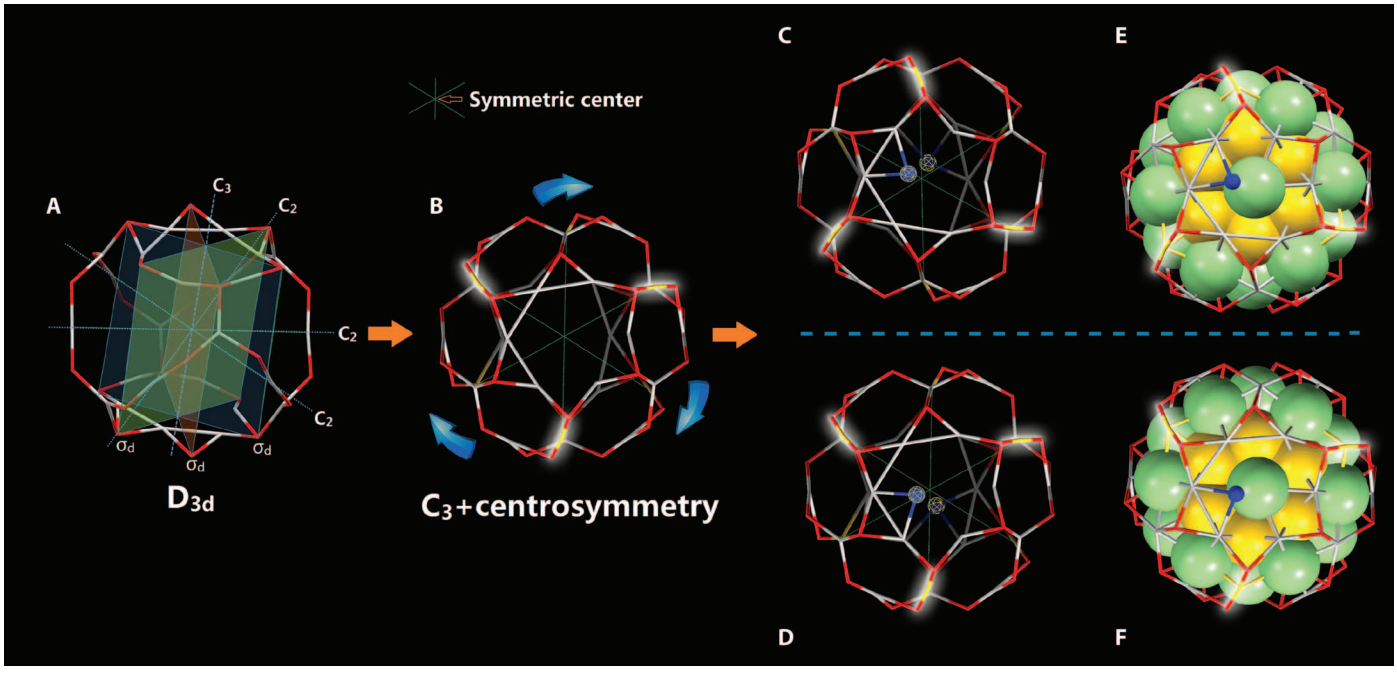

Fig. 3. Chiral structure of $[Ag_{46}Au_{24}(SR)_{32}](BPh_4)_2$ nanocluster. (**A** and **B**) Top view of the shell structure without the AuSR unit and the top/bottom RS group (A) and with the addition of three AuSR groups (B). (**C** and **D**) Top views of two-enantiomer shell. (**E** and **F**) Top views of two-enantiomer nanoclusters without H and C atoms. Gray/green, silver; yellow, gold; red/blue, sulfur.

Table 1. The catalytic performance of CNT-supported metal nanoclusters. Reaction conditions: 20 mg of catalysis, 2 wt % nanocluster loading, 57 μl (0.5 mmol) of styrene, 144 μl (1.5 mmol) of *tert*-butyl hydroperoxide (TBHP), 1.5 ml of ethanol, 65°C, 24 hours.

			Selectivity (%)†		
Entry	**Catalyst**	**Conversion (%)***	**Epoxide**	**Benzaldehyde**	**Other products**
1	Au_{25}/CNT	72.8	20.3	66.4	13.3
2	Ag_{44}/CNT	43.6	6.1	92.6	1.3
3	$Ag_{46}Au_{24}$/CNT	68.2	1.2	96.3	2.5
4	$Ag_{32}Au_{12}$/CNT	69.7	57.6	37.6	4.8
5	CNT	31.7	30.5	55.62	13.88

*Conversion = (styrene converted)/(initial amount of styrene) × 100. †Determined by gas chromatography.

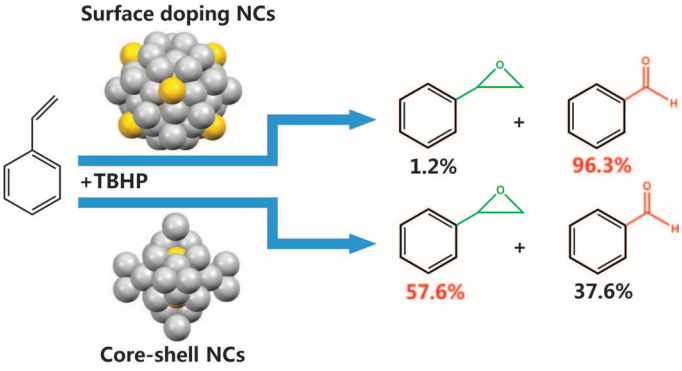

Scheme 1. Two different kinds of nanocluster catalysts in the styrene oxidization. The surface-doped nanocluster (NC) shows high selectivity for benzaldehyde, whereas the core-shell structured nanocluster shows high selectivity for epoxide.

exhibited a better selectivity for benzaldehyde (that is, 92.6%). Compared with the homometal nanoclusters, surface doping bimetallic $Au_{24}Ag_{46}$/CNT (Table 1, entry 3) catalysts could increase the selectivity for epoxide (that is, >95%) and give much better conversion (that is, ~70%) than the homosilver nanocluster does. Therefore, the advantages of both the silver (high selectivity for benzaldehyde) and the gold (high conversion) have been well reflected on the surface doping $Ag_{46}Au_{24}$/CNT catalyst. In contrast, the core-shell structured bimetallic $Ag_{32}Au_{12}$ nanocluster shows a much lower benzaldehyde selectivity (that is, 37.6%) than does the surface doping catalyst. This finding is remarkable in pioneering investigations on the structure effect in atomically precise alloy nanoclusters and demonstrates a clear synergistic effect of the AgAu alloy catalysts (Scheme 1).

In conclusion, we obtained the x-ray crystal structure of a new magic number bimetallic (Au-Ag) nanocluster formulated as $[Ag_{46}Au_{24}(SR)_{32}](BPh_4)_2$ and further investigated its catalytic properties. This nanocluster fills the vacancy between Ag_{44} and Au_{102} nanoclusters. The newly found bimetallic shell holds potential in expanding the library of magic-sized nanoclusters as well as the understanding structure-related properties of thiolate-protected alloy nanoclusters at the atomic level by studying styrene oxidization catalysis.

MATERIALS AND METHODS

The detailed information about the synthesis of $[Ag_{46}Au_{24}(SR)_{32}](BPh_4)_2$ nanocluster is given in the Supplementary Materials. In summary, $AgNO_3$ and $HAuCl_4{\cdot}3H_2O$ were dissolved in methanol to give a yellow turbid liquid. Tertiary butyl was added into the solution to obtain the mixture of Au^I-SR and Ag^I-SR complex. Then, NaOH (1 M) was used to adjust the pH value. After that, $NaBH_4$ was used to reduce this mixture complex. The $Ag_{46}Au_{24}(SR)_{32}^{2+}$ nanoclusters were precipitated out from the solution, washed by hexane, extracted by toluene, and redissolved in CH_2Cl_2 solution. The addition of $NaBPh_4$ (dissolved in methanol) formed $[Ag_{46}Au_{24}(SR)_{32}](BPh_4)_2$ nanocluster. The multiwalled CNT was dispersed in toluene, and a calculated amount (0.1 wt %) of cluster was added to the suspension of CNT under vigorous magnetic stirring. After proceeding overnight, the product was separated from the solution by centrifugation and dried under vacuum for 12 hours. Calcination of the Au_{25}:SR/CNT, Ag_{44}:SR/CNT, and $Ag_{46}Au_{24}$/CNT composites was performed in a quartz-tube oven under vacuum conditions at 200°C for 2 hours to remove the ligands. The detailed method and characterization are available in the Supplementary Materials.

SUPPLEMENTARY MATERIALS

Supplementary material for this article is available at http://advances.sciencemag.org/cgi/content/full/1/7/e1500441/DC1

Materials

Fig. S1. ^1H NMR spectrum of $[Ag_{46}Au_{24}(S^tBu)_{32}](BPh_4)_2$ nanoclusters (single crystal dissolved in CD_2Cl_2).

Fig. S2. Typical TEM images and cluster size distributions of (a) Au_{25}/CNT, (b) Ag_{44}/CNT, (c) $Ag_{32}Au_{12}$/CNT, (d) $Ag_{46}Au_{24}$/CNT before reaction.

Fig. S3. Typical TEM images and cluster size distributions of (a) Au_{25}/CNT, (b) Ag_{44}/CNT, (c) $Ag_{32}Au_{12}$/CNT, (d) $Ag_{46}Au_{24}$/CNT after reaction.

Fig. S4. The digital photo of the $[Ag_{46}Au_{24}(S^tBu)_{32}](BPh_4)_2$ crystals.

Fig. S5. The UV-Vis spectra of (a) $Au_{25}(SC_2H_4Ph)_{18}$–(b)$Ag_{44}(SPhF_2)30^{4-}$; (c) $Ag_{32}Au_{12}(SPhF_2)^{4-}$; (d) $[Ag_{46}Au_{24}(S^tBu)_{32}](BPh_4)_2$ nanoclusters dissolved in dichloromethane solution.

Table S1. Crystal data and structure refinement for $[Ag_{46}Au_{24}(S^tBu)_{32}](BPh_4)_2$ nanoclusters.

Table S2. Atomic coordinates ($\times 10^4$) and equivalent isotropic displacement parameters ($Å^2 \times 10^3$) for $[Ag_{46}Au_{24}(S^tBu)_{32}](BPh_4)_2$.

Table S3. Bond lengths (Å) and angles (°) for $[Ag_{46}Au_{24}(S^tBu)_{32}](BPh_4)_2$ nanoclusters.

Table S4. Anisotropic displacement parameters ($Å^2 \times 10^3$) for $[Ag_{46}Au_{24}(S^tBu)_{32}](BPh_4)_2$.

REFERENCES AND NOTES

1. R. Ferrando, J. Jellinek, R. L. Johnston, Nanoalloys: From theory to applications of alloy clusters and nanoparticles. *Chem. Rev.* **108**, 845–910 (2008).
2. R. Ghosh Chaudhuri, S. Paria, Core/shell nanoparticles: Classes, properties, synthesis mechanisms, characterization, and applications. *Chem. Rev.* **112**, 2373–2433 (2012).
3. S. Link, Z. L. Wang, M. A. El-Sayed, Alloy formation of gold–silver nanoparticles and the dependence of the plasmon absorption on their composition. *J. Phys. Chem. B* **103**, 3529–3533 (1999).
4. T. Pradeep, Anshup, Noble metal nanoparticles for water purification: A critical review. *Thin Solid Films* **517**, 6441–6478 (2009).
5. Y. Sugano, Y. Shiraishi, D. Tsukamoto, S. Ichikawa, S. Tanaka, T. Hirai, Supported Au–Cu bimetallic alloy nanoparticles: An aerobic oxidation catalyst with regenerable activity by visible-light irradiation. *Angew. Chem. Int. Ed.* **52**, 5295–5299 (2013).
6. D. Wang, A. Villa, F. Porta, D. Su, L. Prati, Single-phase bimetallic system for the selective oxidation of glycerol to glycerate. *Chem. Commun.* 1956–1958 (2006).
7. C. L. Bracey, P. R. Ellis, G. J. Hutchings, Application of copper–gold alloys in catalysis: Current status and future perspectives. *Chem. Soc. Rev.* **38**, 2231–2243 (2009).
8. P. Hervés, M. Pérez-Lorenzo, L. M. Liz-Marzán, J. Dzubiella, Y. Lu, M. Ballauff, Catalysis by metallic nanoparticles in aqueous solution: Model reactions. *Chem. Soc. Rev.* **41**, 5577–5587 (2012).
9. S. Xie, H. Tsunoyama, W. Kurashige, Y. Negishi, T. Tsukuda, Enhancement in aerobic alcohol oxidation catalysis of Au_{25} clusters by single Pd atom doping. *ACS Catal.* **2**, 1519–1523 (2012).
10. H. Zhang, T. Watanabe, M. Okumura, M. Haruta, N. Toshima, Catalytically highly active top gold atom on palladium nanocluster. *Nat. Mater.* **11**, 49–52 (2012).
11. L. Kesavan, R. Tiruvalam, M. H. Ab Rahim, M. I. bin Saiman, D. I. Enache, R. L. Jenkins, N. Dimitratos, J. A. Lopez-Sanchez, S. H. Taylor, D. W. Knight, C. J. Kiely, G. J. Hutchings, Solvent-free oxidation of primary carbon-hydrogen bonds in toluene using Au-Pd alloy nanoparticles. *Science* **331**, 195–199 (2011).
12. D. Wang, Y. Li, Bimetallic nanocrystals: Liquid-phase synthesis and catalytic applications. *Adv. Mater.* **23**, 1044–1060 (2011).
13. Z. L. Wang, T. S. Ahmad, M. A. El-Sayed, Steps, ledges and kinks on the surfaces of platinum nanoparticles of different shapes. *Surf. Sci.* **380**, 302–310 (1997).
14. H. Lee, S. E. Habas, S. Kweskin, D. Butcher, A. Somorjai, P. Yang, Morphological control of catalytically active platinum nanocrystals. *Angew. Chem. Int. Ed.* **45**, 7824–7828 (2006).
15. A. U. Nilekar, S. Alayoglu, B. Eichhorn, M. Mavrikakis, Preferential CO oxidation in hydrogen: Reactivity of core–shell nanoparticles. *J. Am. Chem. Soc.* **132**, 7418–7428 (2010).
16. S. Alayoglu, A. U. Nilekar, M. Mavrikakis, B. Eichhorn, Ru–Pt core–shell nanoparticles for preferential oxidation of carbon monoxide in hydrogen. *Nat. Mater.* **7**, 333–338 (2008).
17. M. Chen, D. Kumar, C. Yi, D. W. Goodman, The promotional effect of gold in catalysis by palladium-gold. *Science* **310**, 291–293 (2005).
18. J. W. Hong, D. Kim, Y. W. Lee, M. Kim, S. W. Kang, S. W. Han, Atomic-distribution-dependent electrocatalytic activity of Au–Pd bimetallic nanocrystals. *Angew. Chem. Int. Ed.* **50**, 8876–8880 (2011).
19. P. N. Njoki, W. Wu, P. Lutz, M. M. Maye, Growth characteristics and optical properties of core/alloy nanoparticles fabricated via the layer-by-layer hydrothermal route. *Chem. Mater.* **25**, 3105–3113 (2013).

20. R. Jin, Atomically precise metal nanoclusters: Stable sizes and optical properties. *Nanoscale* **7**, 1549–1565 (2015).
21. S. Yamazoe, K. Koyasu, T. Tsukuda, Nonscalable oxidation catalysis of gold clusters. *Acc. Chem. Res.* **47**, 816–824 (2014).
22. G. Li, R. Jin, Atomically precise gold nanoparticles as new model catalysts. *Acc. Chem. Res.* **46**, 1749–1758 (2013).
23. S. Wang, X. Meng, A. Das, T. Li, Y. Song, T. Cao, X. Zhu, M. Zhu, R. Jin, A 200-fold quantum yield boost in the photoluminescence of silver-doped Ag_xAu_{25-x} nanoparticles: The 13th silver atom matters. *Angew. Chem. Int. Ed.* **53**, 2376–2380 (2014).
24. M. Zhu, C. M. Aikens, M. P. Hendrich, R. Gupta, H. Qian, G. C. Schatz, R. Jin, Reversible switching of magnetism in thiolate-protected Au_{25} superatoms. *J. Am. Chem. Soc.* **131**, 2490–2492 (2009).
25. S. Antonello, N. V. Perera, M. Ruzzi, J. A. Gascón, F. Maran, Interplay of charge state, lability, and magnetism in the molecule-like $Au_{25}(SR)_{18}$ cluster. *J. Am. Chem. Soc.* **135**, 15585–15594 (2013).
26. M. S. Devadas, J. Kim, E. Sinn, D. Lee, T. Goodson III, G. Ramakrishna, Unique ultrafast visible luminescence in monolayer-protected Au_{25} clusters. *J. Phys. Chem. C* **114**, 22417–22423 (2010).
27. S. Park, D. Lee, Synthesis and electrochemical and spectroscopic characterization of biicosahedral Au_{25} clusters. *Langmuir* **28**, 7049–7054 (2012).
28. M. Walter, J. Akola, O. Lopez-Acevedo, P. D. Jadzinsky, G. Calero, C. J. Ackerson, R. L. Whetten, H. Grönbeck, H. Häkkinen, A unified view of ligand-protected gold clusters as superatom complexes. *Proc. Natl. Acad. Sci. U.S.A.* **105**, 9157–9162 (2008).
29. A. Mathew, G. Natarajan, L. Lehtovaara, H. Häkkinen, R. M. Kumar, V. Subramanian, A. Jaleel, T. Pradeep, Supramolecular functionalization and concomitant enhancement in properties of Au_{25} clusters. *ACS Nano* **8**, 139–152 (2014).
30. M. S. Devadas, V. D. Thanthirige, S. Bairu, E. Sinn, G. Ramakrishna, Temperature-dependent absorption and ultrafast luminescence dynamics of bi-icosahedral Au_{25} clusters. *J. Phys. Chem. C* **117**, 23155–23161 (2013).
31. L. Li, H. Liu, Y. Shen, J. Zhang, J. Zhu, Electrogenerated chemiluminescence of Au nanoclusters for the detection of dopamine. *Anal. Chem.* **83**, 661–665 (2011).
32. M. Y. Sfeir, H. Qian, K. Nobusada, R. Jin, Ultrafast relaxation dynamics of rod-shaped 25-atom gold nanoclusters. *J. Phys. Chem. C* **115**, 6200–6207 (2011).
33. I. Dolamic, S. Knoppe, A. Dass, T. Bürgi, First enantioseparation and circular dichroism spectra of Au_{38} clusters protected by achiral ligands. *Nat. Commun.* **3**, 798 (2012).
34. H. Yang, Y. Wang, H. Huang, L. Gell, L. Lehtovaara, S. Malola, H. Häkkinen, N. Zheng, All-thiol-stabilized Ag_{44} and $Au_{12}Ag_{32}$ nanoparticles with single-crystal structures. *Nat. Commun.* **4**, 2422 (2013).
35. C. Kumara, C. M. Aikens, A. Dass, X-ray crystal structure and theoretical analysis of $Au_{25-x}Ag_x(SCH_2CH_2Ph)_{18}^-$ alloy. *J. Phys. Chem. Lett.* **5**, 461–466 (2014).
36. C. Kumara, K. J. Gagnon, A. Dass, X-ray crystal structure of $Au_{38-x}Ag_x(SCH_2CH_2Ph)_{24}$ alloy nanomolecules. *J. Phys. Chem. Lett.* **6**, 1223–1228 (2015).
37. M. Zhu, C. M. Aikens, F. J. Hollander, G. C. Schatz, R. Jin, Correlating the crystal structure of a thiol-protected Au_{25} cluster and optical properties. *J. Am. Chem. Soc.* **130**, 5883–5885 (2008).
38. M. W. Heaven, A. Dass, P. S. White, K. M. Holt, R. W. Murray, Crystal structure of the gold nanoparticle $[N(C_8H_{17})_4][Au_{25}(SCH_2CH_2Ph)_{18}]$. *J. Am. Chem. Soc.* **130**, 3754–3755 (2008).
39. H. Qian, W. T. Eckenhoff, Y. Zhu, T. Pintauer, R. Jin, Total structure determination of thiolate-protected Au_{38} nanoparticles. *J. Am. Chem. Soc.* **132**, 8280–8281 (2010).
40. A. Desireddy, B. E. Conn, J. Guo, B. Yoon, R. N. Barnett, B. M. Monahan, K. Kirschbaum, W. P. Griffith, R. L. Whetten, U. Landman, T. P. Bigioni, Ultrastable silver nanoparticles. *Nature* **501**, 399–402 (2013).
41. B. K. Teo, X. Shi, H. Zhang, Pure gold cluster of 1:9:9:1:9:9:1 layered structure: A novel 39-metal-atom cluster $[(Ph_3P)_{14}Au_{39}Cl_6]Cl_2$ with an interstitial gold atom in a hexagonal antiprismatic cage. *J. Am. Chem. Soc.* **114**, 2743–2745 (1992).
42. G. Li, Z. Lei, Q. Wang, Luminescent molecular Ag–S nanocluster $[Ag_{62}S_{13}(SBu^t)_{32}](BF_4)_4$. *J. Am. Chem. Soc.* **132**, 17678–17679 (2010).
43. S. Jin, S. Wang, Y. Song, M. Zhou, J. Zhong, J. Zhang, A. Xia, Y. Pei, M. Chen, P. Li, M. Zhu, Crystal structure and optical properties of the $[Ag_{62}S_{12}(SBu^t)_{32}]^{2+}$ nanocluster with a complete face-centered cubic kernel. *J. Am. Chem. Soc.* **136**, 15559–15565 (2014).
44. A. Das, C. Liu, H. Y. Byun, K. Nobusada, S. Zhao, N. L. Rosi, R. Jin, Structure determination of $[Au_{18}(SR)_{14}]$. *Angew. Chem. Int. Ed.* **54**, 3140–3144 (2015).
45. S. Chen, S. Wang, J. Zhong, Y. Song, J. Zhang, H. Sheng, Y. Pei, M. Zhu, The structure and optical properties of the $[Au_{18}(SR)_{14}]$ nanocluster. *Angew. Chem. Int. Ed.* **54**, 3145–3149 (2015).
46. A. Das, T. Li, K. Nobusada, C. Zeng, N. L. Rosi, R. Jin, Nonsuperatomic $[Au_{23}(SC_6H_{11})_{16}]^-$ nanocluster featuring bipyramidal Au_{15} kernel and trimeric $Au_3(SR)_4$ motif. *J. Am. Chem. Soc.* **135**, 18264–18267 (2013).
47. D. Crasto, S. Malola, G. Brosofsky, A. Dass, H. Häkkinen, Single crystal XRD structure and theoretical analysis of the chiral $Au_{30}S(S\text{-}t\text{-}Bu)_{18}$ cluster. *J. Am. Chem. Soc.* **136**, 5000–5005 (2014).
48. P. D. Jadzinsky, G. Calero, C. J. Ackerson, D. A. Bushnell, R. D. Kornberg, Structure of a thiol monolayer–protected gold nanoparticle at 1.1 Å resolution. *Science* **318**, 430–433 (2007).
49. C. L. Heinecke, T. W. Ni, S. Malola, V. Mäkinen, O. A. Wong, H. Häkkinen, C. J. Ackerson, Structural and theoretical basis for ligand exchange on thiolate monolayer protected gold nanoclusters. *J. Am. Chem. Soc.* **134**, 13316–13322 (2012).
50. C. Zeng, Y. Chen, K. Kirschbaum, K. Appavoo, M. Y. Sfeir, R. Jin, Structural patterns at all scales in a nonmetallic chiral $Au_{133}(SR)_{52}$ nanoparticle. *Sci. Adv.* **1**, e1500045 (2015).
51. S. Malola, H. Häkkinen, Electronic structure and bonding of icosahedral core-shell gold-silver nanoalloy clusters $Au_{144-x}Ag_x(SR)_{60}$. *J. Phys. Chem. Lett.* **2**, 2316–2321 (2011).
52. M. Zhu, H. Qian, X. Meng, S. Jin, Z. Wu, R. Jin, Chiral Au_{25} nanospheres and nanorods: Synthesis and insight into the origin of chirality. *Nano Lett.* **11**, 3963–3969 (2011).
53. C. Zeng, T. Li, A. Das, N. L. Rosi, R. Jin, Chiral structure of thiolate-protected 28-gold-atom nanocluster determined by X-ray crystallography. *J. Am. Chem. Soc.* **135**, 10011–10013 (2013).
54. Z. Zanolli, R. Leghrib, A. Felten, J. Pireaux, E. Llobet, J. Charlier, Gas sensing with Au-decorated carbon nanotubes. *ACS Nano* **5**, 4592–4599 (2011).

Funding: We acknowledge financial support by the National Natural Science Foundation of China (21072001, 21201005, and 21372006), the Ministry of Education and Ministry of Human Resources and Social Security, the Education Department of Anhui Province, Anhui Province International Scientific and Technological Cooperation Project, and 211 Project of Anhui University. **Author contributions:** S.W. and S.J. conceived and carried out the synthesis and crystallization of the clusters. S.W. and S.Y. conceived and carried out the catalytic reaction. S.C. and Y.S. assisted in the synthesis. J.Z. analyzed the crystal data of the clusters. M.Z. designed the study, supervised the project, analyzed data, and wrote the paper. **Competing interests:** The authors declare that they have no competing interests.

Submitted 8 April 2015
Accepted 10 June 2015
Published 14 August 2015
10.1126/sciadv.1500441

Citation: S. Wang, S. Jin, S. Yang, S. Chen, Y. Song, J. Zhang, M. Zhu, Total structure determination of surface doping $[Ag_{46}Au_{24}(SR)_{32}](BPh_4)_2$ nanocluster and its structure-related catalytic property. *Sci. Adv.* **1**, e1500441 (2015).

Science Advances

Total structure determination of surface doping $[Ag_{46}Au_{24}(SR)_{32}](BPh_4)_2$ nanocluster and its structure-related catalytic property

Shuxin Wang, Shan Jin, Sha Yang, Shuang Chen, Yongbo Song, Jun Zhang and Manzhou Zhu

Sci Adv **1** (7), e1500441.
DOI: 10.1126/sciadv.1500441

Science Advances (ISSN 2375-2548) is published by the American Association for the Advancement of Science, 1200 New York Avenue NW, Washington, DC 20005. The title *Science Advances* is a registered trademark of AAAS.